Applied Catalysis B: Environmental 121–122 (2012) 123–134

Contents lists available at SciVerse ScienceDirect

Applied Catalysis B: Environmental

journal homepage: www.elsevier.com/locate/apcatb

Modulating the copper oxide morphology and accessibility by using micro-/mesoporous SBA-15 structures as host support: Effect on the activity for the CWPO of phenol reaction

Xin Zhong[a,b], Jacques Barbier Jr.[b], Daniel Duprez[b], Hui Zhang[a,*], Sébastien Royer[b,*]

[a] Department of Environmental Engineering, Wuhan University, P.O. Box C319, Luoyu Road, 129#, Wuhan 430079, PR China
[b] Université de Poitiers, CNRS UMR 7285, IC2MP, 4 rue Michel Brunet, 86022 Poitiers Cedex, France

ARTICLE INFO

Article history:
Received 3 February 2012
Received in revised form 28 March 2012
Accepted 1 April 2012
Available online 6 April 2012

Keywords:
SBA-15
*x*CuO/SBA-15(*y*)
Auto-combustion
Catalytic wet peroxide oxidation (CWPO) process

ABSTRACT

This study presents an original approach to the improvement of advanced oxidation process (AOP) efficiencies through the design of highly active catalysts. Then, removal of phenol was obtained under mild conditions by catalytic wet peroxide oxidation (CWPO) process over silica supported micropore and/or mesopore confined copper oxide nanoparticles. The materials, *i.e. y* wt.% CuO (*y* ranging from 4 to 10) on SBA-15 exhibiting different pore structure properties, were entirely characterized. In this study, we took advantage from the evolution of the micropore fraction in the mesoporous silica with the autoclaving temperature of synthesis. While only mesopore nanocasted copper oxide nanoparticle formed when the support exhibits only mesoporosity, micropore silica confined nanoparticles other formed the two supports exhibiting both micropores and mesopores. In this case, mesopore nanocasted nanoparticles can be only observed when copper oxide loading reaches 10 wt.%. As a consequence, the copper active surface is suggested to be higher when copper incorporates interconnected micropores, without limited pore plugging issued from mesopore confined nanoparticle formation.

For the phenol removal reaction, all the materials are exhibiting interesting activity, with a complete conversion of phenol and almost 60–80% of mineralization obtained in less than 2 h at 60 °C. Nevertheless, the results showed that the increase in copper loading up to high values is not needed to achieve high mineralization degree, due to the typical morphology of the materials, *i.e.* confinement of nanoparticles inside micropores or mesopores. In addition, the prepared materials allow a continuous use in reaction with leaching of active phase ($\leq$4.4 mg L^{-1}) which also results in no water post-purification for cation removal as in the case of the classical homogeneous Fenton process.

1. Introduction

The industrial processes generate a wide variety of wastewaters requiring the application of expensive post-treatments. The phenol is a common pollutant found in the effluents coming from various industries. Due to its toxicity and poor biodegradability in conventional wastewater treatment processes, advanced wastewater treatment technologies are needed in order to limit the negative impact on the ecosystems and human health [1]. In contrast to the drawbacks of conventional chemical processes, the effective and economic treatment of hazardous organic pollutants by advanced oxidation processes (AOPs) has attracted continuous interest during the past 20 years [2,3]. Among these techniques, catalytic wet hydrogen peroxide oxidation (CWPO) process allows performing the degradation of many pollutants under mild conditions (20–80 °C and atmospheric pressure), which is considered to be an effective and economical method for treating contaminants [4]. In the typical CWPO process, the redox properties of dissolved transition metal cations (Fe^{2+}, Cu^{2+}) allow generating highly active hydroxyl radicals in the presence of hydrogen peroxide. However, the homogeneous systems usually need precise reaction pH value (usually around 3). In addition, the removal of metals sludge produced during the reaction requires additional separation steps, resulting in increased overall costs [5,6]. In order to overcome the major drawbacks of the homogeneous process, *i.e.* the elimination of homogeneous transition metal catalyst, heterogeneous processes have been paid great attention and recently played a key role in the CWPO processes in mild reaction conditions [7–15].

Recently, several copper- and iron-based heterogeneous systems have been reported to be efficient catalysts for the CWPO

* Corresponding authors.
E-mail addresses: eeng@whu.edu.cn (H. Zhang), sebastien.royer@univ-poitiers.fr (S. Royer).

0926-3373/$ – see front matter © 2012 Elsevier B.V. All rights reserved.
http://dx.doi.org/10.1016/j.apcatb.2012.04.002

processes (Table 1). The highest efficiency over iron-based systems is obtained when the reaction is performed under acidic conditions. Compared to iron-based catalyst for CWPO of phenol compound, Cu-based catalysts play a similar role but reaction can be performed at near neutral pH value with high efficiency. The Fe- and Cu-active phases were supported or incorporated over a wide variety of materials, including mesoporous silica [16–20], zeolites [21–27], alumina [28–30], active carbon [13,31–35], clays [36–40] and perovskites [41,42]. Unfortunately, the major drawbacks of these systems are (i) a limited activity per mol of transition metal, and (ii) a catalyst stability in reaction which is affected by either the active phase or the support properties. Activity and stability then not only strongly depend on the active phase environment, but also on the reaction conditions (temperature, pH, *etc.*) (Table 1). Hence, attempts have been made to improve either catalytic activity, by increasing dispersion, or catalyst stability, by changing transition metal–support interaction of these heterogeneous systems [43–46].

Since the discovery of ordered mesoporous silica materials in 1992 [47], a rapid development of the field allowed the production of numerous materials, siliceous [48–51], or non-siliceous [52–54], having different pore structure properties. As one of the most popular ordered mesoporous silica, the SBA-15 structure presenting a *P6mm* type pore symmetry, has attracted special attention because of its highly ordered structure, easily controlled pore size, high specific surface area [55–57] and obviously higher hydrothermal stability than other structures like MCM-41 [58,59]. The pore size of the ordered mesoporous materials was reported to be ranging from 2 to 10 nm with narrow pore size distribution depending on different synthesis processes. In addition, a further increase in pore size, up to 30 nm and larger, is possible using swelling agent [60]. The narrow pore size distribution and large pore diameter channels could enable to make the pollutants easy accessible to the pore channel in order to overcome the diffusion restriction. Unfortunately, a too large pore size increase results in the decrease of surface area or the deformation of the hexagonal structure [61]. Another advantage of the SBA-15 type silica is the possibility to modulate the fraction of residual micropore in the inorganic walls of the mesoporous structure [62–64]. Such a microporosity can be a great advantage for the formation of accessible nanosized particles, allowing an increase of the active phase dispersion. All these properties indicate that SBA-15 of properly designed pore morphology, maintaining a well-ordered mesoporous structure, is a suitable support for the immobilization of active sites.

In this study, mesoporous SBA-15 silica supported copper nanoparticles materials were synthesized *via* a simple and efficient procedure involving the impregnation of a glycine–nitrate complex on preformed silica, followed by combustion step. This method, *i.e.* the *in situ* auto-combustion method, was found to be efficient to produce homogeneous nanocomposite [6,43,45]. Different copper loadings were prepared in mesoporous silica presenting different pore diameters and micropore fractions in order to achieve highly dispersed copper nanoparticle formation either in the mesopores or in the micropores. Indeed, it is well known that the mesoporous SBA-15 structure can present some residual microporosity, and this microporosity can be a great advantage to achieve high dispersion, due to the physical crystal growth limitation if particles are located inside or at the mouth of these micropores. In addition, SBA-15 possessing mesoporosity and microporosity not only plays an important role in dispersing CuO particles, but can also facilitate the accessibility of reactants to the active phase. Then, these materials were used for the phenol CWPO reaction. The effects of the operational parameters were carefully analyzed in phenol oxidation using hydrogen peroxide in mild conditions to evidence the positive effect of the heterogenization of the process. The optimal pH value for copper species as the active species is around 4–7

Table 1
Short survey of recent studies on copper/iron oxide nanoparticles in structured supports for CWPO reactions.

Catalyst	Catalytic activity conversion/TOC removal	Metal leaching ($mg L^{-1}$)	Reaction conditions	Refs.
Fe_2O_3/SBA-15 (10.2 wt.%)	X_{phenol} = 100%, TOC = 55%	8.2	Catalyst 0.5 $g L^{-1}$, 5 × 10^{-4} mol L^{-1} phenol, 100 mM H_2O_2, flow rate 2 $L h^{-1}$, 40 °C, 3 h, pH 3.7	[6]
CuO/SBA-15 (20 wt.%)	TOC = 85%	20	Phenol 54.2 mM, 0.6 $g L^{-1}$ catalyst, 29.4 mM H_2O_2, pH_0 5.5 (not buffered), 1 MPa (air pressure), 100 °C, 0.33 h	[16]
Fe_2O_3/SBA-15 (16 wt.%)	TOC = 58%	6		
Fe/Cu/SBA-15 (12.2 wt.% Fe; 7.5 wt.% Cu)	TOC = 65%	0.9 for Fe; 15.9 for Cu		
Cu-HMS	X_{phenol} = 32.7% Identified intermediates[a]: CAT/HQ/BQ	–	Catalyst 0.05 g, 10 mmol phenol, 20 mmol H_2O_2, 10.8 g H_2O, 60 °C, pH 7, 4 h	[17]
Cu-SBA-15	X_{phenol} = 41.9–59.4% CAT/HQ/BQ			
Copper/MFI zeolites	X_{phenol} = 40%, TOC = 31%	0.6	5 × 10^{-5} mol phenol, 0.1 g catalyst, 0.1 N H_2O_2, atmospheric pressure, 25 °C	[21]
Cu/ZSM-5	X_{phenol} = 70%	–	Catalyst 0.1 $g L^{-1}$, 10 mM phenol, 100 mM H_2O_2, 60 °C, 3 h reaction time	[22]
CuO/Al_2O_3 (1 wt.%)	X_{phenol} = 100%, TOC = 80%	9.7	pH 7, 3 $g L^{-1}$, 1000 mg L^{-1} phenol, 150 °C, 180 min	[28]
CuO/alumina	TOC = 48%	pH > 4, 4; pH < 4, 17	1 $g L^{-1}$ phenol, 180 min, 50 °C, catalyst 25 $g L^{-1}$, 1 dose of 3.3 mL H_2O_2	[29]
CuO/activated carbon (4.6 wt.%)	X_{phenol} = 100%, TOC = 70%	–	1000 mg L^{-1} phenol, one step 0.1 M H_2O_2 addition, 1 g 4.6 wt.% CuO-catalyst, 180 min, 80 °C	[31]

[a] CAT is short for catechol; BQ is short for benzoquinone; HQ is short for hydroquinone.

[65]. In this case, the pH value was maintained at 6.5 by buffer solution, near to the neutral pH condition which is adequate and easily applied in most wastewater and prevents from large amount of copper leaching in the acid conditions. In addition, effects of copper loading, and especially the localization of copper nanoparticles (in micropores or in mesopores), is investigated and discussed. Furthermore, the stability of the copper active species, which is also a crucial parameter, was also evaluated.

2. Experimental

2.1. Materials

All chemicals required to prepare the mesoporous SBA-15 silica and derived copper catalysts were used as purchased: tetraethylorthosilicate ($Si(OC_2H_5)_4$, TEOS, 98%, Aldrich), non-ionic triblock co-polymer Pluronic P123 (poly(ethylene oxide)-*block*-poly(propylene oxide)-*block*-poly(ethylene oxide), $EO_{20}PO_{70}EO_{20}$, molecular weight = 5800, BASF Corp.), hydrochloric acid and copper nitrate ($Cu(NO_3)_2{\cdot}2.5H_2O$, 98%, Aldrich). For the CWPO reaction, the chemicals were also used as purchased without further purification: phenol (C_6H_5OH, Sigma–Aldrich) and buffer solution (Na_2HPO_4, NaH_2PO_4, Sigma–Aldrich).

2.2. Synthesis of SBA-15 support and xCuO/SBA-15(y) catalysts

The SBA-15 supports, presenting pore size from 6 nm to 10 nm, were prepared according to previously published procedure [46]. A mass of 12 g of triblock copolymer P123 is dissolved in 360 g of water and 32 g of HCl 37 wt.%. The solution is heated at 35 °C to allow the complete dissolution of the copolymer. 25 g of TEOS is thereafter slowly added under vigorous stirring. The solution is stirred at 35 °C for 24 h, and then transferred in a Teflon-line autoclave for treatment at 50 °C (in order to achieve 6 nm pore size, SBA-15(6) sample), 100 °C (for pore size at 8 nm, SBA-15(8) sample) and 140 °C (for pore size at 10 nm, SBA-15(10) sample) for 24 h. After hydrothermal treatment, the autoclave is cooled down to room temperature and the solid filtered, washed and dried at 80 °C overnight. Before use and characterization, supports are calcined under air at 550 °C for 4 h (temperature increase rate = 1 °C min^{-1}).

*x*CuO/SBA-15(*y*) catalysts, where *x* is the metallic copper content and *y* is the pore size of the silica support, are prepared by the *in situ* auto-combustion method, as previously described [43,45]. In a typical synthesis, 0.117 g of $Cu(NO_3)_2{\cdot}2.5H_2O$ (for 4 wt.% loading) is first dissolved in 20 mL of distilled water, and glycine added as complexing agent (the mass of glycine weighted is obtained by fixing the ratio $(NO_3)^-$/glycine equal to 1). After 4 h of aging, the glycine–nitrate solution is mixed with 1.0 g of freshly calcined SBA-15(*y*) support, and water slowly evaporated under mixing at 100 °C. When a dry powder is obtained, the temperature is increased up to 280 °C for glycine auto-ignition [*CAUTION*: glycine combustion is highly exothermic and projection of hot matter can occur during combustion step]. Finally, copper–silica composites are calcined at 600 °C for 4 h in order to remove any residual carbonaceous matter from the catalyst (temperature increase rate = 1 °C min^{-1}).

2.3. Physico-chemical characterization

*x*CuO/SBA-15(*y*) catalysts are systematically characterized by ICP-OES, XRD at low and high angles, nitrogen physisorption and TEM analysis.

The chemical composition (Si/Cu) of the catalysts is determined using a sequential scanning inductively coupled plasma optical emission spectrometer (ICP-OES) from Perkin, after adequate dissolution of the samples under microwave heating.

Powder XRD patterns are collected on a Bruker AXS D5005 X-ray diffractometer, using a Cu Kα radiation (λ = 1.54184 Å) as X-ray source and equipped with a SolX-type detector. For low angle analysis, patterns are recorder for 2θ from 0.8° to 3° by 0.01° per step (step time = 10 s). For large angle analysis, patterns are recorded for 2θ from 15° to 80° by 0.05° per step (step time = 2 s).

Nitrogen physisorption was carried out at −196 °C on Autosorb 1-MP (Quantachrome) apparatus. Prior to N_2 physisorption, the samples were degassed under vacuum at 300 °C for at least 6 h. Value of surface area (S_{BET}) is determined by the 10 point BET method. The total pore volume (V_{pore}) is determined on the plateau of the adsorption branch at P/P_0 = 0.97. The pore size, D_{BJH}, is evaluated using the Barret–Joyner–Halenda method applied to the adsorption branch. Finally, the micropore volume (V_{micro}) is determined by the *t*-plot method.

Information concerning support and copper particle size and localization are obtained by transmission electronic microscopy (TEM). The micrographs were collected on a JEOL 2100 instrument (operated at 200 kV with a LaB_6 source and equipped with a Gatan Ultra scan camera).

2.4. Catalytic tests

Catalytic tests are performed under mild conditions (atmospheric pressure and 60 °C) in a thermostated reactor of 250 mL continuously stirred, using phenol as reactant and hydrogen peroxide as oxidant. It was initially verified that no external and internal diffusional resistances occur, and that the reaction is performed in kinetic regime. The reaction pH value is maintained at 6.5 by adding buffer solution during the reaction. In a typical experiment, 100 mL of phenol aqueous solution was prepared with an initial concentration of 200 mg L^{-1}, and given amounts of hydrogen peroxide and catalyst were added at reaction time = 0 min. Reaction solution is sampled at fixed time intervals. These samples are mixed with 0.1 g of manganese oxide for at least 15 min to eliminate residual H_2O_2, and filtered by 0.22 μm membranes before measuring the residual phenol concentration and TOC content. Phenol concentration was determined using a high performance liquid chromatography (Thermofinnigan HPLC) equipped with an Aminex HPX-87 (Biorad) column. The total organic carbon (TOC) content was measured by a 1020A Bioritech TOC meter. Copper leaching was systematically evaluated by ICP analyses by quantification of the dissolved copper concentration in the solution after test using ICP-OES, as previously described. The variation of H_2O_2 concentration with reaction time is measured by colorimetry after complexation of hydrogen peroxide with vanadate salt, using a UV spectrophotometer (Secomam, RS232).

3. Results and discussion

3.1. The SBA-15(y) supports

Since the properties of the SBA-15 silica supports are extensively described in the literature, and as described in our previous works [6,43,45], the *in situ* autocombustion method does not strongly alter the support pore structure, the properties of the SBA-15(*y*) samples are only gathered in Table 2 and shortly described below.

The small-angle XRD patterns of the supports (not shown) exhibit three easily observable reflections at low 2θ, indexable as the (d_{100}), (d_{110}) and (d_{200}) reflections, which is characteristic of a highly ordered hexagonal mesoporous structure of *P6mm* symmetry. The reflections are however progressively shifting to the lower 2θ by increasing the autoclaving temperature, which is confirmed by the increase in d_{100} and a_0 in Table 2. Consequently, the increase in autoclaving temperature results in an increase in cell parameter.

Table 2
Physico-chemical properties of the SBA-15 supports and the copper-based catalysts.

Sample	Cu content (wt.%)	S_{BET} ($m^2\,g^{-1}$)	V_{pore} ($cm^3\,g^{-1}$)	V_{micro} ($cm^3\,g^{-1}$)	d_{100} (nm)	a_0 (nm)	D_p (nm)
SBA-15(10)	–	486	1.2	0.058	8.9	10.3	10.9
SBA-15(8)	–	694	0.86	0.12	7.1	8.2	7.3
SBA-15(6)	–	510	0.47	0.10	6.7	7.8	5.7
4CuO/SBA-15(10)	4.1	447	1.07	0.052	10.0	11.5	11.2
4CuO/SBA-15(8)	4.1	626	0.79	0.090	9.1	10.5	7.3
4CuO/SBA-15(6)	4.1	469	0.47	0.078	7.8	9.0	5.7
6CuO/SBA-15(10)	6.5	442	1.04	0.049	9.4	10.8	11.2
10CuO/SBA-15(10)	10.8	433	1.03	0.035	9.5	10.9	11.3
10CuO/SBA-15(8)	10.8	534	0.726	0.069	8.7	10.0	7.4
10CuO/SBA-15(6)	10.8	473	0.456	0.087	7.5	8.7	5.7

CuO content in wt.%: as determined by ICP-OES analysis; V_{pore}: mesopore volume measured at $P/P_0 = 0.97$; V_{micro}: micropore volume calculated from *t*-plot; D_p: BJH average pore size calculated on the adsorption branch; a_0: unit-cell parameter determined from the position of the (1 0 0) diffraction peak ($a_0 = d_{100} \times 2/\sqrt{3}$).

The surface areas of the supports are found to vary between 486 $m^2\,g^{-1}$ and 694 $m^2\,g^{-1}$, the highest being measured for the SBA-15(8) sample prepared at intermediate temperature. As awaited, the mean pore size is found to increase with the hydrothermal treatment temperature applied during the synthesis. Consequently, the lowest pore size is obtained after autoclaving at 50 °C [SBA-15(6)] and the highest is obtained after autoclaving at 140 °C [SBA-15(10)]. The increase in pore size is accompanied by an increase in pore volume, which is found to reach 1.2 $cm^3\,g^{-1}$ over SBA-15(10). All these values and trends are in agreement with those previously obtained over similar materials.

Finally, the micropore volume is found to slightly increase from 0.1 $cm^3\,g^{-1}$ to 0.12 $cm^3\,g^{-1}$ when temperature of autoclaving increases from 50 °C to 100 °C, and then decreases up to 0.06 $cm^3\,g^{-1}$ when autoclaving temperature reaches 140 °C. The contribution of the micropore volume to the total surface area explains why the surface area is found to increase and then to decrease with the autoclaving temperature. In addition, this evolution of micropore volume is consistent with the complete description of the pore properties of the SBA-15 type materials given by Galarneau et al. [62,63] and more recently by Kleitz et al. [64]. Indeed, the synthesis temperature dependent topology of the SBA-15 system is well known, which is clearly described as originating from the micellar behavior of non-ionic surfactants as P123 [45,46]. This effect is ascribed to the increased temperature during the hydrothermal treatment leading to (i) increased pore size and (ii) decreased initial unconnected ultramicroporosity (below 80 °C) to connected supermicroporosity or small mesopore (around 100 °C) and finally to no or only a few microporosity and formation of a second bridging mesoporosity having size similar to the main pore channels (around 130 °C) [6,46]. Consequently, the peculiar properties of the pore structure described as: (i) unconnected micropore + small mesopore; (ii) connected micropore + medium mesopore; and (iii) large mesopore + second bridging mesopore, can be advantageously used to increase the dispersion of an active phase such as CuO by confining a part of it inside the micropores.

3.2. Characterization of xCuO/SBA-15(y) nanocomposites

3.2.1. X-ray diffraction results

XRD patterns at low and high angles for the calcined *x*CuO/SBA-15(*y*) materials are depicted in Fig. 1. The small-angle XRD patterns (Fig. 1A–C for selected materials) of the catalysts always exhibit three diffraction peaks at low 2θ, which indicates that organized pore structure is always maintained after the auto-combustion process. Only a slight shift of the reflections can be observed, and as can be observed in Table 2, the CuO formation in the pores results in a small increase in cell parameter. Nevertheless, the addition of precursor and its further decomposition into copper oxide by self-combustion do not result in pore structure collapse.

The wide angle X-ray diffraction patterns are given in Fig. 1D–F. Large differences can be observed depending on the support used.

- On SBA-15(10) (Fig. 1D): The peaks at $2\theta = 35.5°$ and 38.7° thus indicating that the presence of monoclinic CuO (JCPDS 048-1548), and the relative intensity of the peaks is found to increase with the increase in copper loading. The average crystal size of CuO, calculated from the Scherrer equation after Warren's correction for instrument broadening, was about 22 ± 0.5 nm whatever the loading is. This clearly shows that the crystal size is not affected by the copper loading which is consistent with a thermal stabilization of the nanoparticles by confining effect of the particles in the large meso-channels, even if crystal size of CuO is larger than that of the pore size of initial support [45].
- On SBA-15(6) and (8) (Fig. 1E and F): At low CuO loading, the peaks at $2\theta = 35.5°$ and 38.7° characteristic of the monoclinic CuO phase (JCPDS file n° 048-1548) are hardly detected compared to over the SBA-15(10) support. Due to the similar content for the three materials, this result can only be explained by: (i) the maintaining of copper oxide in an amorphous state, or (ii) a reduction of the particle size down to the detection limit of the instrument. When loading increase up to 10 wt.% of Cu, CuO reflections are becoming easily detected for the 10CuO/SBA-15(8) while they remain poorly defined and of weak intensity for the 10CuO/SBA-15(6).

The main difference between these two last samples and the previous one concerns the micropore fraction on the total pore volume. Indeed, SBA-15(6) and SBA-15(8) present higher micropore content than the SBA-15(10). Thus, the localization of the CuO cluster in the microporosity of the support will obviously result in the decrease in the CuO reflection intensity due to the limited size of the clusters formed.

3.2.2. Physical properties evolution

The nitrogen adsorption/desorption isotherms are presented in Fig. 2, and the textural characteristics are gathered in Table 2.

It can be observed that all the *x*CuO/SBA-15(*y*) samples present isotherms of type IV, with H1-type hysteresis loops type (parallel adsorption and desorption branch, characteristic for cylindrical pores). The shape of the loop seems to be unchanged after the CuO formation, indicating that catalysts exhibit uniform cylindrical porosity (compare curves (a), (b), and (c) in Fig. 2, corresponding to 4CuO/SBA-15(6), 6CuO/SBA-15(6) and 10CuO/SBA-15(6) materials, respectively). This result is in agreement with the previously presented XRD results, with the maintaining of clearly identified low angle 2θ reflections.

Then, the main evolutions concern the values of textural properties. Indeed, the curves are found to shift down along the *y*-axis with the increase in copper loading. This is clearly characteristic of a decrease in pore volume, as summarized in Table 2. This

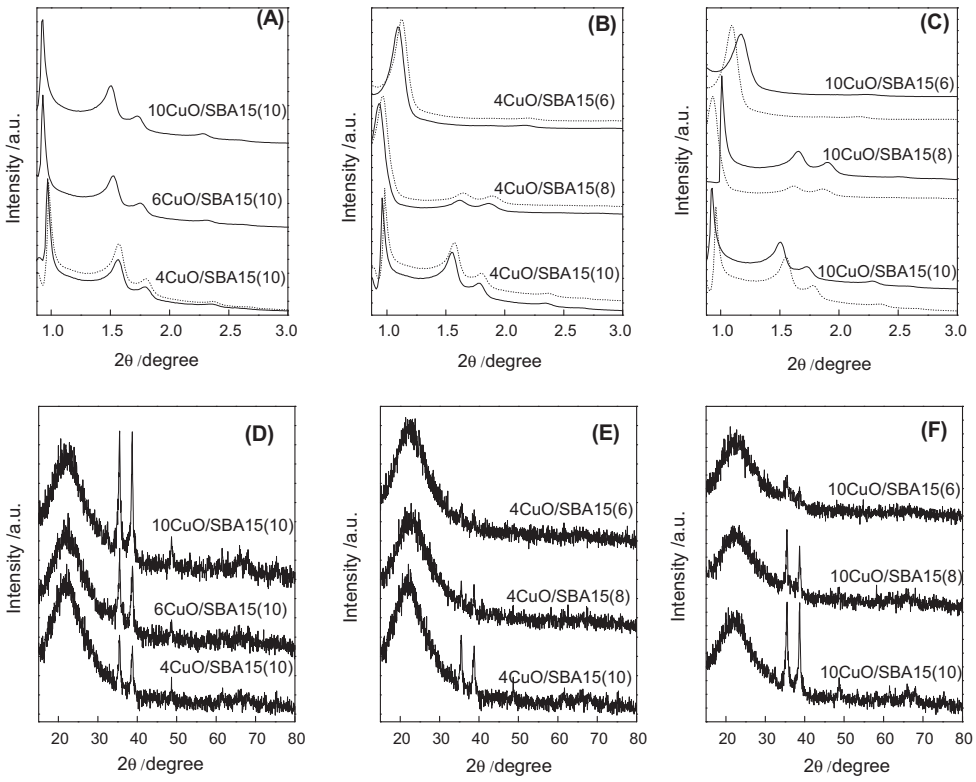

Fig. 1. XRD patterns of selected *x*CuO/SBA-15(*y*) materials: (A–C) low angles patterns; (D–F) high angles patterns.

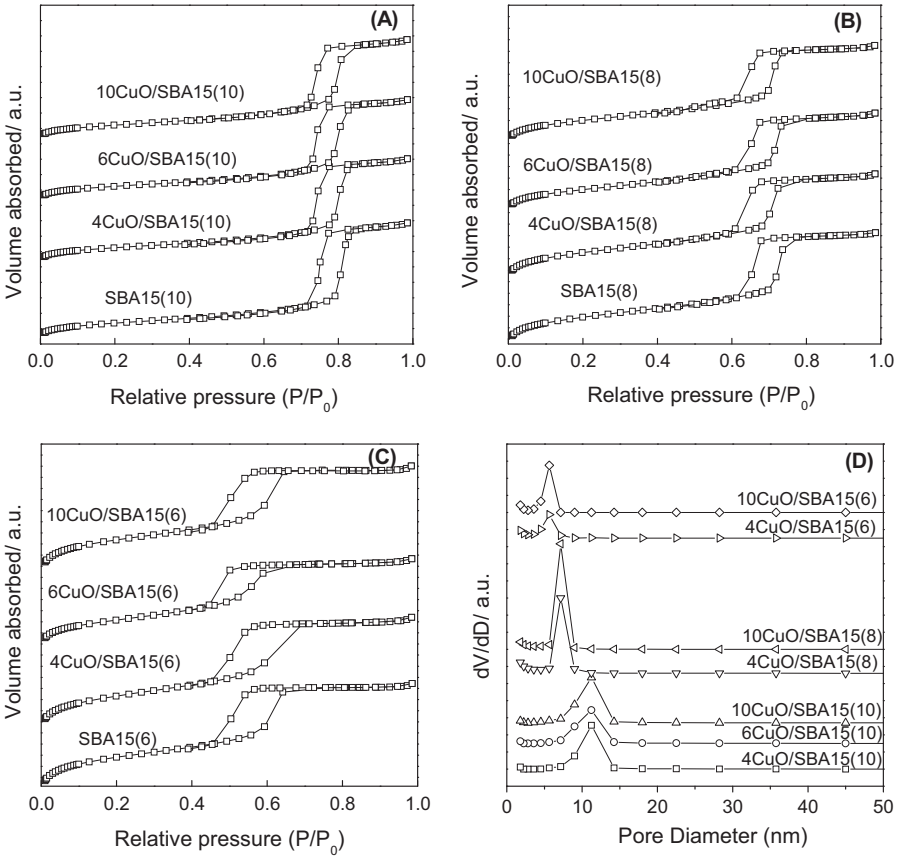

Fig. 2. N_2 adsorption–desorption isotherms obtained for the *x*CuO/SBA-15(*y*) materials.

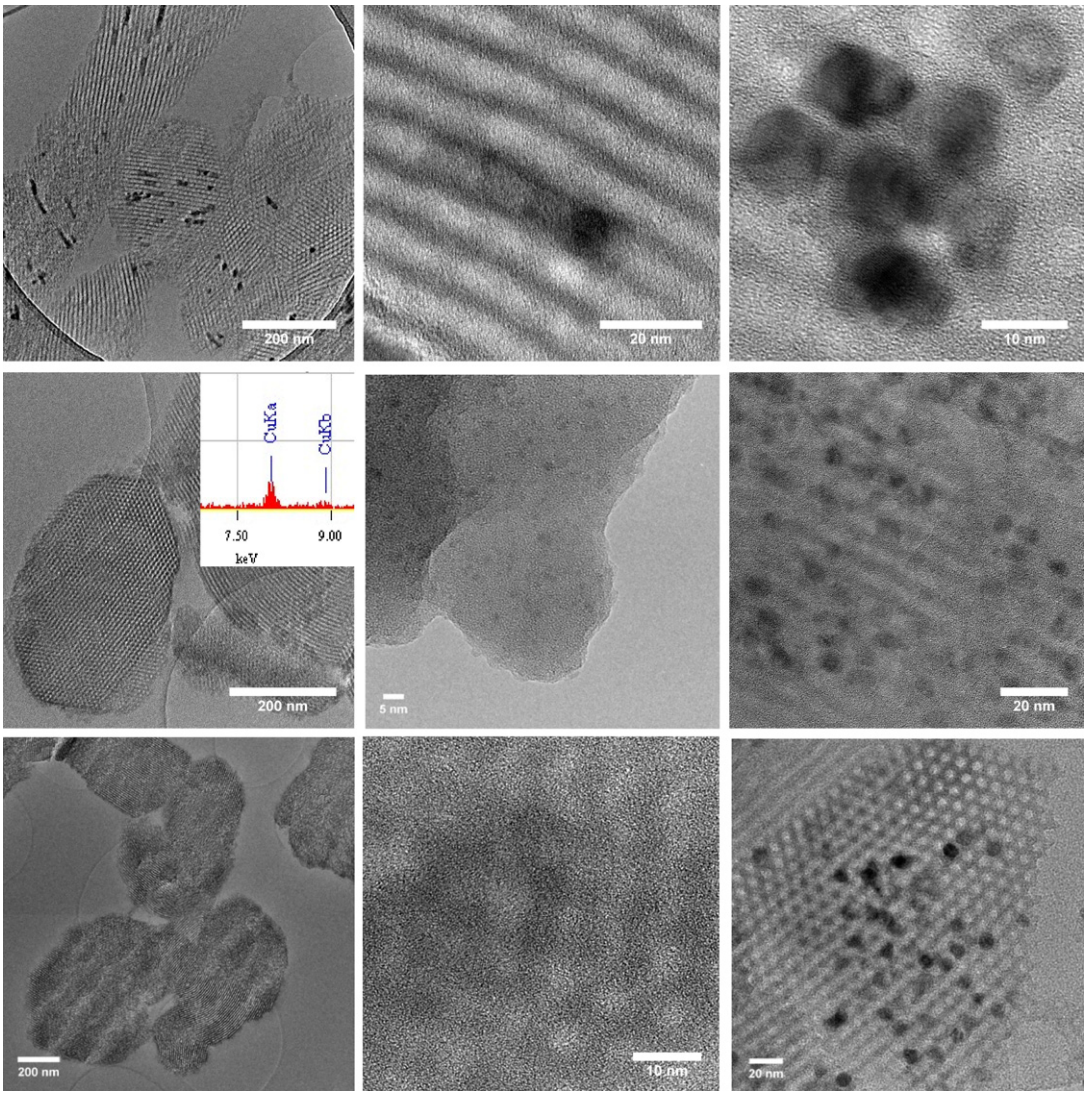

Fig. 3. Representative TEM images of *x*CuO/SBA-15(*y*) selected materials: (A–C) 4CuO/SBA-15(10) sample; (D and E) 4CuO/SBA-15(6) and (F) 10CuO/SBA-15(6); (G and H) 4CuO/SBA-15(8) and (I) 10CuO/SBA-15(8).

evolution can however be explained by the filling of the pores by the CuO phase. In addition, surface area is found to decrease with the increase in CuO loading while the mean pore size is only a few altered whatever the loading or the initial support.

The pore volume and pore size of the catalyst play a key role during the catalytic reaction, especially in liquid phase. Indeed, if the pore size is not enough larger than the geometric size of the molecule to be converted, the contact of the pollutant and the active site will be minimized to the external surface. An important part of the active sites will be inaccessible into the mesopore and possibly in proximity of the micropore surface, giving *in-fine* a decrease in catalyst efficiency. An optimal mesopore size of the support would favor the diffusion of the molecules in the pore, up to the active sites, while the confining of the CuO particles in the micropores in close proximity of the mesopore surface will obviously lead to high reaction rates. In our case, the mesopore size of the support, from 6 nm to 10 nm, is large enough for the diffusion of a small molecule like phenol (having a geometric size ~0.66 nm) [66].

3.2.3. Copper oxide morphology

Representative TEM images of selected *x*CuO/SBA-15(*y*) samples are depicted in Fig. 3. First, the TEM images supported the maintenance of the hexagonal pore structure whatever the silica support and the CuO loading. Indeed, the channel-like pore organizations, as well as the hexagonal arrays of pore, are clearly identified on the images. Nevertheless, large differences in CuO particle morphology and size can be observed depending on the initial support. The main observations are:

- On SBA-15(10) support (Fig. 3A–C): copper particles are mainly observed in the form of small particles confined in the mesopore whatever the loading. The particles are in the form of crystalline CuO tubes, with diameter close to the pore size of the support and variable length from ~10 nm to 50–100 nm. Focus on the CuO nanotubes shows that the tube is aggregates of crystals. As suggested by the XRD analysis, the CuO loading increase does not allow observing any change in CuO particle morphology and size, whose remain similar. In this case, a careful analysis of the material does not allow detecting very small particle, *i.e.* of size largely lower than the pore size.

On the two other supports, SBA-15(6) and SBA-15(8): at low loading, the formation of mesopore confined aggregate of CuO particles which is more difficult to observe. Example of large zone empty of confined aggregates is presented in Fig. 3D and G for the two low loadings. Then, a lowest pore plugging is suggested, as

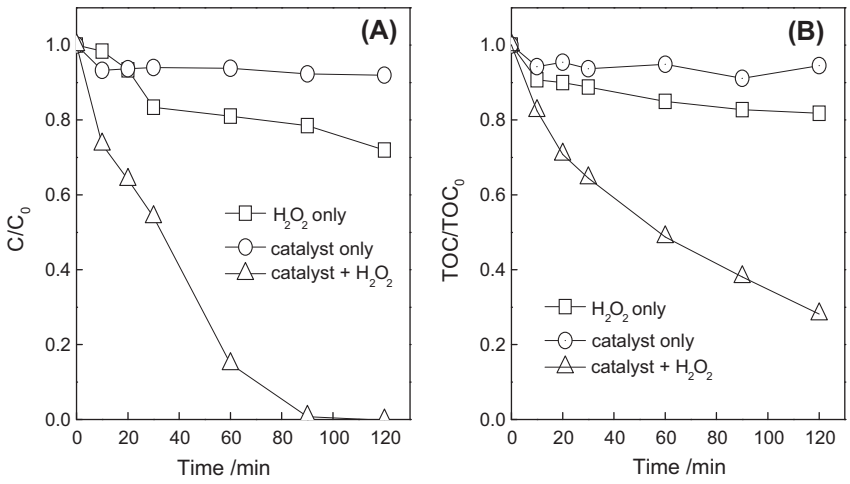

Fig. 4. Phenol conversion (A) and TOC removal (B) obtained at 60 °C with hydrogen peroxide alone (blank), catalyst alone (adsorption test), and hydrogen peroxide and catalyst (catalytic degradation); reaction conditions: phenol 200 mg L^{-1}; H_2O_2 concentration 0.05 mol L^{-1}; catalyst 4CuO/SBA-15(8); loading 0.5 g L^{-1}.

experimentally observed by N_2-physisorption. EDXS analysis on these zones however shows that Cu is present (shown in Fig. 3D for the 4CuO/SBA-15(6) sample), and high magnification observation with increased contrast (Fig. 3E and H) shows that CuO forms as very small CuO particles (at size largely lower than the pore size of the support). Nevertheless, some formation of mesopore confined particles can be observed in low extent, which can explain why XRD reflections ascribed to CuO are detected. The increase in CuO loading (Fig. 3E and I) allows an easy detection of the mesopore confined aggregates in these two materials. Thus, the formation of these ~10 nm diameter aggregates is responsible for the XRD reflections observed in Fig. 1F.

3.3. CWPO of phenol over xCuO/SBA-15(y)

3.3.1. Role of the heterogeneous catalyst

The evaluation of the catalytic activity in phenol oxidation by *x*CuO/SBA-15(*y*) was carried out under different experimental conditions. To investigate the contribution of catalyst adsorption and H_2O_2 oxidation to the reaction, the phenol conversion and TOC removal are carried out by only hydrogen peroxide (H_2O_2 oxidation) and only catalysts (catalyst adsorption) (Fig. 4). From this picture, the results showed that: (i) in the presence of *x*CuO/SBA-15(*y*) catalyst alone, *i.e.* without oxidant, results in very limited phenol conversion and TOC removal, (ii) phenol removal is also negligible with hydrogen peroxide alone (without catalyst), (iii) a large increase in phenol conversion and TOC abatement is observed when catalyst and H_2O_2 are present. Then, Fig. 4 highlights the efficiency of the heterogeneous catalytic system to activate the reaction. Then, the catalyst presents a limited adsorption capacity (even if the surface of the catalyst is high), but is able to produce highly active hydroxyl radicals which can react with phenol. Consequently, 4CuO/SBA-15(8) catalyst and H_2O_2 allow achieving phenol conversion and TOC removal of 100% and 71.2% after 120 min of reaction, respectively.

It can be concluded that the conversion of the H_2O_2 molecules into free radicals played the key role in the reaction which would greatly promote the phenol degradations in the CWPO process [29,31,67,68]. In a homogeneous catalytic reaction, free radicals are produced, thanks to the redox metallic ions in solution [69],

$$H_2O_2 + M^{n+} \rightarrow M^{(n+1)+} + HO^{\bullet} + OH^- \quad (1)$$

As studied by other authors [17,70], in the heterogeneous catalytic reaction, the active phase (copper oxide – CuO) reacts with hydrogen peroxide, resulting in the generation of hydroxyl ($^{\bullet}OH$) radicals leading to the degradation of phenol molecules. The catalyst then affects the global reaction rate through the rate of radical formation:

$$S\text{–}Cu^{2+} + H_2O_2 \rightarrow S\text{–}Cu^{1+} + HO_2^{\bullet} + H^+ \quad (2)$$

$$S\text{–}Cu^{1+} + H_2O_2 \rightarrow S\text{–}Cu^{2+} + OH^{\bullet} + OH^- \quad (3)$$

Table 3
Selected reaction results and catalyst stability for the CWPO of phenol. Reaction conditions: catalyst: 0.5 g L^{-1}; phenol: 200 mg L^{-1}; H_2O_2 concentration = 0.05 mol L^{-1}.

Sample	X_{phenol} (%)	TOC (%) ($X_{H_2O_2}$ (%))	Cu^{2+} in solution (mg L^{-1})		Cu leaching (%)
Blank (homogeneous with 4 mg L^{-1} of Cu^{2+})	31.2	28.7	–		–
4CuO/SBA-15(10)	100	67.3 (48.1)	3.2		9.7
4CuO/SBA-15(8)-1	100	71.4 (73.6)	10 min	3.3	12.5
			30 min	3.3	
			60 min	3.3	
			90 min	3.8	
			120 min	4.1	
4CuO/SBA-15(8)-2	94.7	68.9	3.7		10.7
4CuO/SBA-15(8)-3	85.8	61.2	3.1		9.5
4CuO/SBA-15(6)	83.2	60.8 (43.7)	3.9		11.8
6CuO/SBA-15(10)	100	80.5	4.4		8.4
10CuO/SBA-15(10)	100	84.2	3.6		4.1
10CuO/SBA-15(8)	100	81.8	3.7		4.2
10CuO/SBA-15(6)	100	79.3	3.5		4.0

X_{phenol} and TOC: phenol conversion and TOC abatement after 2 h of reaction; $X_{H_2O_2}$: hydrogen peroxide conversion; 4CuO/SBA-15(8)-1, -2 and -3: catalyst used for one, two and three successive tests; Cu^{2+} in solution/mg L^{-1}: copper content in the solution at the end of the reaction; Cu leaching (%): percentage of copper leached from the catalyst at the end of the reaction.

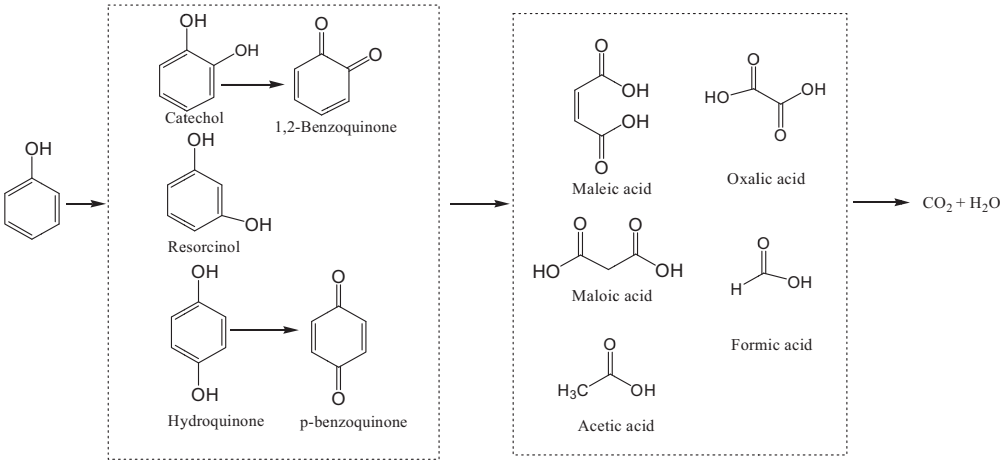

Scheme 1. Identification of the main intermediates and residual compounds in solution during the CWPO reaction.

where S represents accessible redox surface sites of the heterogeneous catalyst and M represents the metallic ions.

The higher catalytic activity of 4CuO/SBA-15(8) than that of homogeneous Cu^{2+} catalytic system ($[Cu^{2+}] = 4\,mg\,L^{-1}$) evidenced that active phase on the surface of catalyst has a great influence on the reaction rate (Fig. 7 and Table 3).

The reaction mechanism for the oxidation of phenol has been previously studied, and main identified intermediates are described in Scheme 1 [15,17,68,69,71]. As the •OH radicals are generated by the interaction between the hydrogen peroxide molecule and the CuO active site, the first step of phenol degradation is the generation of aromatic compounds which causes the solution color to turn into dark brown. These intermediates, such as catechol, hydroquinone and resorcinol, are given in Scheme 1. The attack of the aromatic rings by •OH radical leads to partial oxidation. The above organic compounds later underwent ring broken down to generate some by-products including maleic acid, oxalic acid, formic acid, malonic acid and acetic acid. Finally, the degradation of these compounds during reaction leads to CO_2 and H_2O formation. Some of the intermediates, mainly the short-chain organic acids such as oxalic acid, are however refractory to the oxidation. This can explain why residual TOC remains in the effluent.

3.3.2. *Influence of hydrogen peroxide concentration and catalyst loading on phenol oxidation reaction*

In the CWPO reaction, the concentration of oxidant is essential to the reaction, which directly conditioned the concentration of active radicals produced for the phenol degradation (active radicals identified in Eqs. (2) and (3)). The effect of hydrogen peroxide concentration is evaluated by increasing the hydrogen peroxide concentration from 0.01 to 0.1 mol L^{-1} while maintaining the phenol concentration and catalyst loading as constants (Figs. S1 and S2). Fig. 5A–C summarizes the effect of hydrogen peroxide concentration, catalyst loading and copper loading in SBA-15 support on the TOC removal efficiency in the CWPO reaction. According to the catalytic test results, TOC abatement is increasing with increasing H_2O_2 concentration (Fig. 5A) and catalyst loading (Fig. 5B). The overall stoichiometry for the complete mineralization of phenol by H_2O_2 can be written as follows [12]:

$$C_6H_5OH + 14H_2O_2 \rightarrow 6CO_2 + 17H_2O \quad (4)$$

According to the overall stoichiometry for the complete degradation of phenol by H_2O_2, 14 mol of H_2O_2 are theoretically needed to completely convert 1 mol of phenol into CO_2. In the present study, when 0.01 or 0.025 mol L^{-1} was added into 100 mL of phenol solution (at a concentration of 200 mg L^{-1}), *i.e.* below the overall stoichiometry, phenol conversion and TOC abatement remain limited (Fig. S1). At H_2O_2 dosage of 0.05 mol L^{-1}, the H_2O_2/phenol molar ratio is about 23.5. This value is 1.8 times larger than the theoretical value to completely convert phenol into carbon dioxide. Nevertheless, while a complete conversion of phenol is observed after 90 min, TOC abatement is not complete and residual carbon remains in the solution (Fig. S1). This is due to the fact that the H_2O_2 may (i) undergo the thermal decomposition during reaction (15% decomposition in pure water at 60 °C). However, this decomposition remains limited compared to the decomposition in presence of catalyst; (ii) act as scavenger over a certain concentration (as described by Eqs. (5) and (6)); (iii) lead to stable by-products in solution, which is responsible for the residual TOC.

$$HO^{\bullet} + H_2O_2 \rightarrow HO_2^{\bullet} + H_2O \quad (5)$$

$$HO^{\bullet} + HO_2^{\bullet} \rightarrow O_2 + H_2O \quad (6)$$

As can be seen in Fig. 5A, TOC removal efficiency increased linearly with the increase of H_2O_2 dosage until 0.05 mol L^{-1}. However, further increase in H_2O_2 dosage did not give great improvement in TOC removal efficiency which remains incomplete.

Defining the efficiency of hydrogen peroxide as:

$$x = \left[\frac{\Delta TOC\ (mg\ L^{-1})}{\Delta TOC_{th}\,(mg\ L^{-1})}\right] \quad (7)$$

where ΔTOC_{th} is the theoretical TOC abatement if all H_2O_2 is consumed to convert the phenol according to Eq. (4), and ΔTOC is the experimental TOC abatement.

The efficiency of hydrogen peroxide decreases with the increase in H_2O_2 concentration (Fig. 5A), indicating that hydrogen peroxide becomes less efficient for the organic molecule oxidation while its initial concentration is increasing. The results indicate, as described previously, that complete TOC abatement cannot be achieved even at high H_2O_2 initial concentration, and that some by-products in solution are produced during reactions. These by-products are mainly refractory molecules (Scheme 1), such as short-chain acids, that are difficult to oxidize.

3.3.3. *Impact of the support porosity and copper morphology on the catalytic activity*

The pore size of a catalyst and the active phase dispersion are key factors determining the final catalytic performance of a material. The phenol conversion and TOC abatement and H_2O_2 concentration evolutions with reaction time are plotted in Fig. 6 for catalysts having different pore diameters and residual microporosity fractions. More than the mesopore size which is high enough to ensure

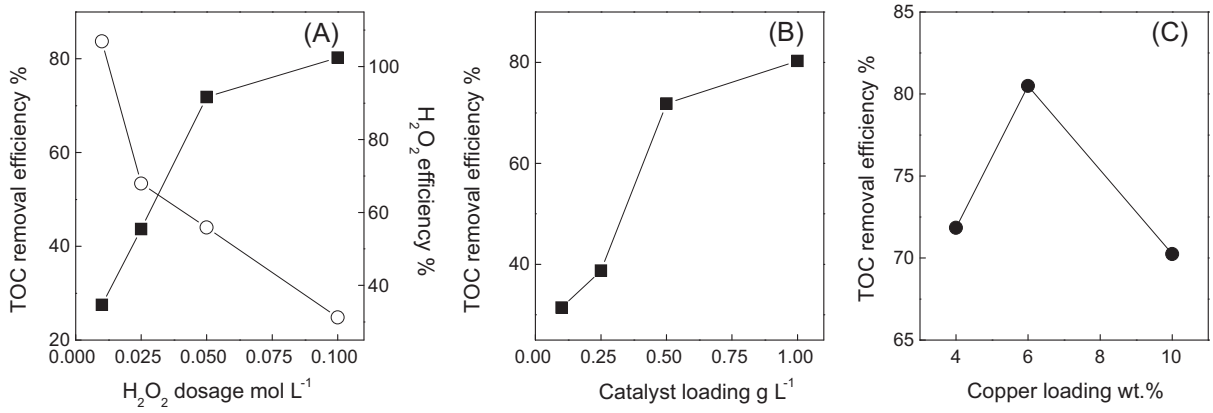

Fig. 5. Effect of H_2O_2 concentration (A), catalyst loading (B) and copper loading (C) on TOC removal efficiency during the CWPO reaction. Reaction conditions: (A) 4CuO/SBA-15(8) catalyst at 0.5 g L^{-1}; phenol 200 mg L^{-1}; (B) phenol 200 mg L^{-1}, H_2O_2 concentration 0.05 mol L^{-1}, 4CuO/SBA-15(8) catalyst; (C) phenol 200 mg L^{-1}, H_2O_2 concentration 0.05 mol L^{-1}, *x*CuO/SBA-15(8) catalyst at 0.5 g L^{-1}.

an easy diffusion of phenol in the catalyst pores, the dispersion of the copper oxide was observed to be strongly affected by microporosity fraction in the material (see XRD in Fig. 1E and TEM in Fig. 3).

At the end of the 120 min of reaction, the lowest phenol conversion, TOC abatement and H_2O_2 conversion are obtained for the 4CuO/SBA-15(6) material, 83.2%, 60.8% and 43.7%, respectively. The highest activity is measured for the 4CuO/SBA-15(8) material which exhibits phenol conversion, TOC abatement and H_2O_2 conversion of 100%, 71.4% and 73.6%, respectively. Then, catalytic activity increases with mesopore diameter of the support, up to 8 nm, and then decreased with further increase of pore diameter up to 10 nm. Normally, increasing the pore diameter of the catalyst should promote the diffusion of pollutant molecules to the active sites, which should result in better catalytic performance [61]. Such evolution is not observed in our case. Although the pore diameter is large enough for the diffusion of phenol to the active sites (dynamic diameter of phenol is ~0.66 nm), the copper dispersion is found to strongly vary depending on the support synthesis conditions. Indeed, Kleitz et al. [64] reported a clear description of the microporosity and interconnectivity between mesopores in SBA-15 hexagonal type silica. Then, at low autoclaving temperature (typically 50 °C), the pore structure of SBA-15 consists in small mesopores (~6 nm in our case) and residual microporosity. However, they suggest no connection between the mesopores. At intermediate temperature (100 °C in our case), pore structure consists in medium mesopores (8 nm) with a secondary small mesopore network for interconnection, and a fraction of residual micropores. Finally, at high temperature (140 °C), the pore network consists in interconnected large mesopore. Analysis of the copper morphology and localization in the materials prepared in this study confirm the possibility to achieve small CuO particles (size lower than the pore size) formation in the materials containing microporosity and/or small mesoporosity of interconnection (case of 4CuO/SBA-15(6) and 4CuO/SBA-15(8)). The formation of such small particles is not observed on the support synthesized at high temperature (140 °C), 4CuO/SBA-15(10), for which only CuO particle plugging mesopores are observed. Then, the large crystal and aggregate formation in 4CuO/SBA-15(10) plugging the mesopore can explain why a slightly lowest activity is obtained on this material compared to this of the 4CuO/SBA-15(8). Indeed, this last material is presenting CuO in the form of fine and dispersed nanoparticles, as schematized in Scheme 2. Due to the lower crystal size and localization, a highest concentration of copper active size is obtained, resulting in higher catalytic activity. Nevertheless, the 4CuO/SBA-15(6) material in which small particles also formed is presenting the lowest activity. However, this material is, in the model proposed by Kleitz et al. [64], the only one in which

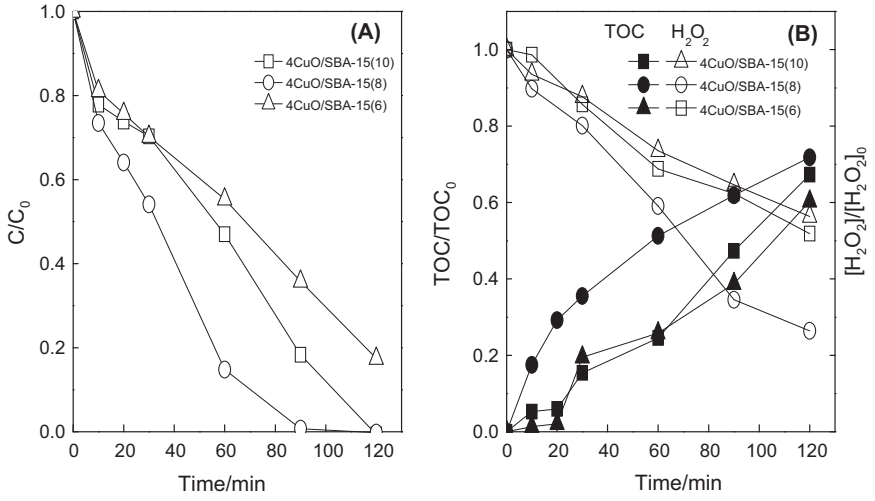

Fig. 6. Effect of pore size of the support on the phenol conversion (A) and TOC abatement and H_2O_2 consumption (B) during the CWPO reaction. Reaction conditions: catalyst 0.5 g L^{-1}; phenol 200 mg L^{-1}; H_2O_2 concentration 0.05 mol L^{-1}.

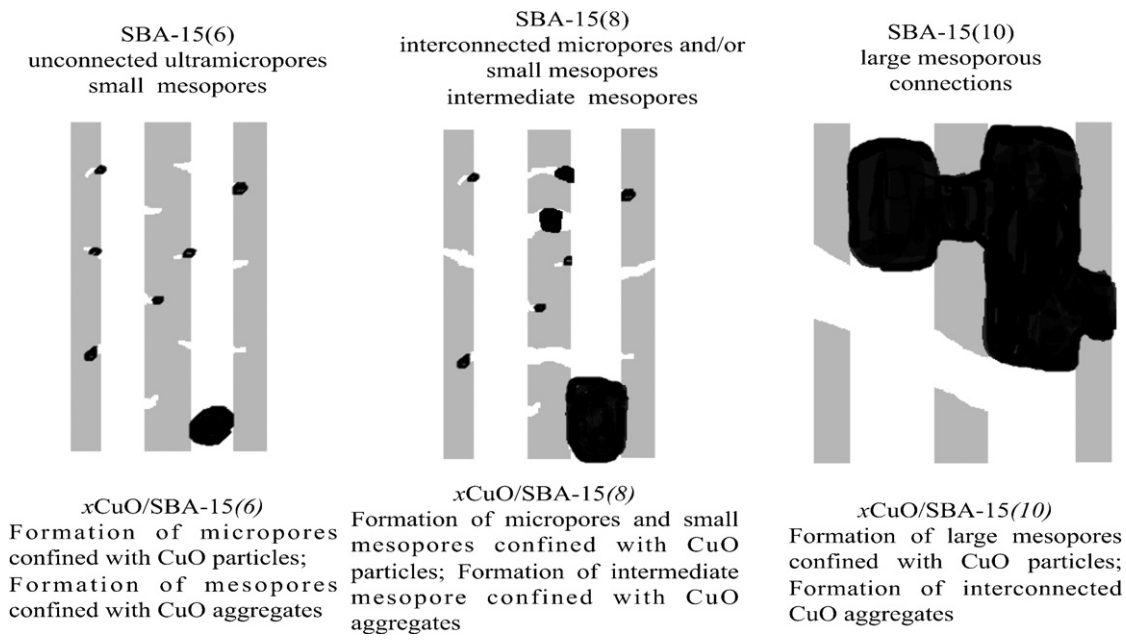

Scheme 2. Evolution of the CuO cluster size and localization along with the morphology of the SBA-15 host support at the micro and meso-scales.

mesopores are not interconnected (Scheme 2). Consequently, the lack of mesopore interconnection and the possible resulting diffusional resistances in the mesopores issued from this can be one reason of the lower activity measured for this material. To conclude, the optimal pore diameter of 8 nm to maximize the catalytic activity is not only originating from increased mass transfer of phenol in the silica porosity but probably results from a compromise between mesopore interconnection and reduced CuO crystal size leading to higher accessible active surface and limited mesopore plugging.

This interpretation is confirmed by the effect of the CuO loading in the silica porosity on the catalytic activity (Table 3, Fig. 5C and Fig. S3). From Fig. 5C, the rate of phenol degradation increases with the increase in copper loading on SBA-15(8) from 4 wt.% to 6 wt.%, and then decreased for 10 wt.%. Then, while the 10CuO/SBA-15(8) catalyst presents the highest copper loading, the lowest phenol conversion rate is measured (Fig. S3). This means that the efficiency of this last solid in radical formation is lower than for 4- and 6CuO/SBA-15(8) materials – in other words, this material is exhibiting a lower copper surface site concentration. A similar evolution is observed on the TOC abatement curves (Fig. S3) with an efficiency order following: 6CuO/SBA-15(8) > 4CuO/SBA-15(8) > 10CuO/SBA-15(8). Nevertheless, this activity evolution can be explained by the evolution in CuO particle size and localization in the silica porosity. At low copper loading (4 wt.% and 6 wt.%), the copper oxide particles are observed to be in the form of very fine particles with no visible pore plugging (Fig. 3D and E). By increasing the copper loading up to 10 wt.%, crystalline particles having size close to the pore size of the support are observed to form (Fig. 3F) which will result in more consequent pore plugging. Due to this pore plugging, the accessibility of the copper surface active site will then decrease, giving *in-fine* a lower catalytic activity than over materials having lower CuO loading but exhibiting highest copper dispersion (case of 4- and 6CuO/SBA-15(8) materials).

It is then clearly demonstrated that the catalytic activity is strongly related to the copper accessible active site which depends on the initial support pore properties (micro- and meso-scales) and copper loading. Indeed, the presence of secondary small mesopore network or micropore allows achieving better CuO dispersion with a possible crystal growth limitation by confining effect. In addition to an increased copper surface developed, the localization in the microporosity resulted in limited mesopore plugging. All these parameters allow achieving higher activity than over a solid in which CuO particles grow in the mesopores.

3.3.4. Stability of the xCuO/SBA-15(y) catalysts and copper leaching

Investigation of catalyst stability is of crucial importance for the CWPO process in long-term reactions. Due to the pH of work, CuO in copper-containing heterogeneous catalysts is reported to slowly dissolve. This copper elution is clearly observed whatever the material used for reaction, with a Cu content in the solution at the end of the test almost constant at 3.2–4.4 mg L^{-1}. While this value is low, it however corresponds to a Cu leaching from the catalyst from a few percent (~4%, for 10 wt.% loading) to more than 10% [case of 4CuO/SBA-15(8)] which confirmed the limited stability in reaction of these materials. It is observed, by quantifying the Cu^{2+} content in solution at different reaction times that copper oxide quickly dissolves. An almost constant value in solution is then obtained after only 10 min (case of 4CuO/SBA-15(8)-1 experiment, Table 3). This limited stability in reaction is however a well-known problem of these copper-based systems, but also of the Fe-based ones (Table 1, values of leaching depend on the active phase and the reaction conditions, *e.g.* temperature, pH...). Nevertheless, the measured efficiencies are in all case largely higher than this measured for a homogeneous reaction under similar conditions. Indeed, homogeneous system using Cu^{2+} at 4 mg L^{-1} in the solution leads to only 31.3% of phenol conversion, much lower than that of the *x*CuO/SBA-15(*y*) materials as catalysts. Then, the heterogeneous system strongly impacts the phenol degradation rate and is necessary for the achievement of high TOC abatement.

In addition, tests of reusability show that the heterogeneous systems suffer from progressive activity decrease. Fig. 7 and Table 3 summarize the evolution of the catalytic performance of the 4CuO/SBA-15(8) material after one, two and three reaction cycles. Then, phenol conversion is observed to progressively decrease with the number of cycles, due to the progressive elution of copper from the catalyst. However, the phenol conversion still remains high, indicating maintaining of good performances after three runs even if the CuO phase is observed to dissolve whatever the cycle (Cu^{2+} in solution always at 3–4 ppm at the end of each test, Table 3). XRD

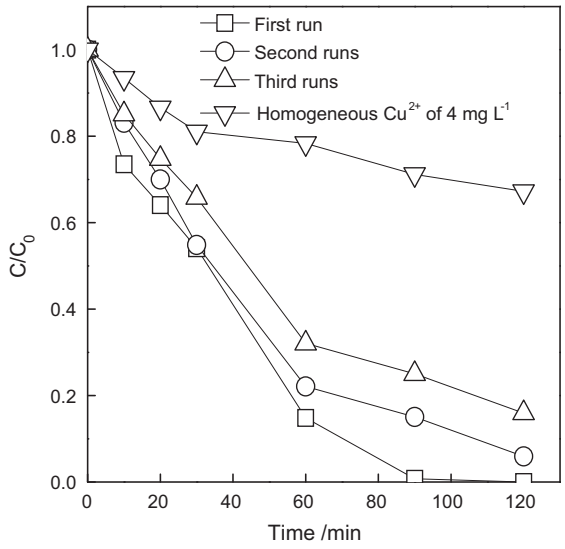

Fig. 7. Evaluation of the catalyst stability and comparison with homogeneous CWPO reaction. Reaction conditions: catalyst 0.5 g L^{-1}; phenol 200 mg L^{-1}; H_2O_2 concentration 0.05 mol L^{-1}.

spectra of used samples (Fig. S4) evidenced that the pore structure remained unchanged after the oxidation reaction. The wide angle analysis however showed that the peak characteristic of the CuO phase is becoming less intense. The decrease in intensity can however be explained by the leaching of the CuO phase during the test. To conclude, the systems present a good reusability (no strong poisoning of the active sites, and no silica pore structure collapse), until sufficient copper contents are maintained in the catalyst.

4. Conclusions

The catalytic wet hydrogen peroxide oxidation of phenol was studied in a batch reactor using copper-based SBA-15 catalysts under mild conditions. The use of SBA-15 type silica synthesized under different conditions, and then exhibiting different pore structure properties, allow to evidence that the catalytic activity of the *x*CuO/SBA-15(*y*) catalyst is influenced by the copper dispersion and accessibility to the active sites on the surface of the support. When silica presents mainly large mesopore (synthesized at high hydrothermal treatment temperature), mesopore confined CuO particles are generated. However, this material is presenting lower catalytic activity that materials in which small copper oxide nanoparticles form, probably confined in the secondary small mesopore network or micropore. Stability study shows a steady stability of these systems, since a part of copper leaches from the catalyst. However, a high catalytic activity can be maintained after successive cycles even if it slightly decreases. Consequently, the heterogeneous catalytic process may be regarded as a promising •OH based heterogeneous systems for the oxidative degradation of organic contaminants in wastewater, if sufficient active phase stabilization can be achieved.

Acknowledgements

X. Zhong greatly acknowledges the Chinese Science Council for two year research grant (No. 20106050) at the University of Poitiers, France and academic award for excellent Ph.D. Candidates funded by Ministry of Education of China (No. 5052011205013). We appreciate the financial support by the Fundamental Research Funds for the Central Universities, China (Grant No. 201120502020004) and Natural Science Foundation of China (Grant No. 20977069). Sébastien Royer acknowledges the CNRS for his 6 months delegation.

Appendix A. Supplementary data

Supplementary data associated with this article can be found, in the online version, at doi:10.1016/j.apcatb.2012.04.002.

References

[1] G. Busca, S. Berardinelli, C. Resini, L. Arrighi, Journal of Hazardous Materials 160 (2008) 265–288.
[2] M. Pera-Titus, V. Garcia-Molina, M.A. Banos, J. Gimenez, S. Esplugas, Applied Catalysis B: Environmental 47 (2004) 219–256.
[3] I. Oller, S. Malato, J.A. Sanchez-Perez, Science of the Total Environment 409 (2011) 4141–4166.
[4] S. Zrncevic, Z. Gomzi, Industrial and Engineering Chemistry Research 44 (2005) 6110–6114.
[5] N. Al-Hayek, J.P. Eymery, M. Dore, Water Research 19 (1985) 657–666.
[6] L. Xiang, S. Royer, H. Zhang, J.M. Tatibouet, J. Barrault, S. Valange, Journal of Hazardous Materials 172 (2009) 1175–1184.
[7] J. Barrault, C. Bouchoule, K. Echachoui, N. Frini-Srasra, M. Trabelsi, F. Bergaya, Applied Catalysis B: Environmental 15 (1998) 269–274.
[8] G. Centi, S. Perathoner, T. Torre, M.G. Verduna, Catalysis Today 55 (2000) 61–69.
[9] N. Crowther, F. Larachi, Applied Catalysis B: Environmental 46 (2003) 293–305.
[10] J.G. Mei, S.M. Yu, J. Cheng, Catalysis Communications 5 (2004) 437–440.
[11] T.L.P. Dantas, V.P. Mendonça, H.J. Jose, A.E. Rodrigues, R.F.P.M. Moreira, Chemical Engineering Journal 118 (2006) 77–82.
[12] A. Rey, M. Faraldos, J.A. Casas, J.A. Zazo, A. Bahamonde, J.J. Rodriguez, Applied Catalysis B: Environmental 86 (2009) 69–77.
[13] A. Dhaouadi, N. Adhoum, Applied Catalysis B: Environmental 97 (2010) 227–235.
[14] Y. Zhan, X. Zhou, B. Fu, Y. Chen, Journal of Hazardous Materials 187 (2011) 348–354.
[15] S. Zhou, Z. Qian, T. Sun, J. Xu, C. Xia, Applied Clay Science 53 (2011) 627–633.
[16] J.A. Melero, G. Calleja, F. Martinez, R. Molina, Catalysis Communications 7 (2006) 478–483.
[17] L. Wang, A. Kong, B. Chen, H. Ding, Y. Shan, M. He, Journal of Molecular Catalysis A: Chemical 230 (2005) 143–150.
[18] N. Gokulakrishnan, A. Pandurangan, P.K. Sinha, Industrial, Engineering Chemistry Research 48 (2009) 1556–1561.
[19] P. Shukla, S. Wang, H. Sun, H.M. Ang, M. Tade, Chemical Engineering Journal 164 (2010) 255–260.
[20] J.A. Melero, G. Calleja, F. Martinez, R. Molina, M.I. Pariente, Chemical Engineering Journal 131 (2007) 245–256.
[21] S. Valange, Z. Gabelica, M. Abdellaoui, J.M. Clacens, J. Barrault, Microporous and Mesoporous Materials 30 (1999) 177–185.
[22] K. Maduna Valkaj, A. Katovic, S. Zrncevic, Journal of Hazardous Materials 144 (2007) 663–667.
[23] H. Kusic, N. Koprivanac, I. Selanec, Chemosphere 65 (2006) 65–73.
[24] R. Gonzalez-Olmos, U. Roland, H. Toufar, F.D. Kopinke, A. Georgi, Applied Catalysis B: Environmental 89 (2009) 356–364.
[25] S. Navalon, M. Alvaro, H. Garcia, Applied Catalysis B: Environmental 99 (2010) 1–26.
[26] R. Prihodko, I. Stolyarova, G. Gunduz, O. Taran, S. Yashnik, V. Parmon, V. Goncharuk, Applied Catalysis B: Environmental 104 (2011) 201–210.
[27] R. Gonzalez-Olmos, F. Holzer, F.D. Kopinke, A. Georgi, Applied Catalysis A: General 398 (2011) 44–53.
[28] S.K. Kim, K.H. Kim, S.K. Ihm, Chemosphere 68 (2007) 287–292.
[29] N. Inchaurrondo, J. Cechini, J. Font, P. Haure, Applied Catalysis B: Environmental 111–112 (2011) 641–648.
[30] N. Al-Hayek, M. Dore, Water Research 24 (1990) 973–982.
[31] R.M. Liou, S.H. Chen, Journal of Hazardous Materials 172 (2009) 498–506.
[32] T.D. Nguyen, N.H. Phan, M.H. Do, K.T. Ngo, Journal of Hazardous Materials 185 (2011) 653–661.
[33] M.A. Fontecha-Camara, M.A. Alvarez-Merino, F. Carrasco-Marin, M.V. Lopez-Ramon, C. Moreno-Castilla, Applied Catalysis B: Environmental 101 (2011) 425–430.
[34] X. Hu, B. Liu, Y. Deng, H. Chen, S. Luo, C. Sun, P. Yang, S. Yang, Applied Catalysis B: Environmental 107 (2011) 274–283.
[35] F. Duarte, F.J. Maldonado-Hodar, L.M. Madeira, Applied Catalysis B: Environmental 103 (2011) 109–115.
[36] D. Tabet, M. Saidi, M. Houari, P. Pichat, H. Khalaf, Journal of Environmental Management 80 (2006) 342–346.
[37] H. Hassan, B.H. Hameed, Chemical Engineering Journal 171 (2011) 912–918.
[38] M. Luo, D. Bowden, P. Brimblecombe, Applied Catalysis B: Environmental 85 (2009) 201–206.
[39] E.G. Garrido-Ramirez, B.K.G. Theng, M.L. Mora, Applied Clay Science 47 (2010) 182–192.
[40] L. Alejandro Galeano, A. Gil, M. Angel Vicente, Applied Catalysis B: Environmental 104 (2011) 252–260.
[41] J.L. Sotelo, G. Ovejero, F. Martínez, J.A. Melero, A. Milieni, Applied Catalysis A: General 47 (2004) 281–294.

[42] J. Faye, E. Guelou, J. Barrault, J.M. Tatibouet, S. Valange, Topics in Catalysis 52 (2009) 1211–1219.
[43] D. Sellam, M. Bonne, S. Arrii-Clacens, G. Lafaye, N. Bion, S. Tezkratt, S. Royer, P. Marecot, D. Duprez, Catalysis Today 157 (2010) 131–136.
[44] J. Gu, Y. Huang, S.P. Elangovan, Y. Li, W. Zhao, I. Toshio, Y. Yamazaki, Ji Shi, Journal of Physical Chemistry C 115 (2011) 21211–21217.
[45] A. Ungureanu, B. Dragoi, A. Chirieac, S. Royer, D. Duprez, E. Dumitriu, Journal of Materials Chemistry 21 (2011) 12529–12541.
[46] M. Bonne, D. Sellam, J.P. Dacquin, A.F. Lee, K. Wilson, L. Olivi, A. Cognigni, P. Marecot, S. Royer, D. Duprez, Chemical Communications 47 (2011) 1509–1511.
[47] C.T. Kresge, M.E. Leonowicz, W.J. Roth, J.C. Vartuli, J.S. Beck, Nature 359 (1992) 710–712.
[48] P.T. Tanev, T.J. Pinnavaia, Science 267 (1995) 865–867.
[49] C. Chen, W.J. Son, K.S. You, J.W. Ahn, W.S. Ahn, Chemical Engineering Journal 161 (2010) 46–52.
[50] F. Kleitz, S.H. Choi, R. Ryoo, Catalysis Communications (2003) 2136–2137.
[51] Y. Xia, H. Dai, H. Jiang, L. Zhang, Catalysis Communications 11 (2010) 1171–1175.
[52] Y. Izumi, K. Asakura, Y. Iwasawa, Journal of Catalysis 127 (1991) 631–644.
[53] S. Bernal, J.J. Calvino, M.A. Cauqui, J.M. Gatica, C. Larese, J.A. Perez Omil, J.M. Pintado, Catalysis Today 50 (1999) 175–206.
[54] M. Bonne, S. Pronier, Y. Batonneau, F. Can, X. Courtois, S. Royer, P. Marecot, D. Duprez, Journal of Materials Chemistry 20 (2010) 9205–9214.
[55] D. Zhao, Q. Huo, J. Feng, B.F. Chmelka, G.D. Stucky, Journal of the American Chemical Society 120 (1998) 6024–6036.
[56] Q. Tang, S. Hu, Y. Chen, Z. Guo, Y. Hu, Y. Chen, Y. Yang, Microporous and Mesoporous Materials 132 (2010) 501–509.
[57] D. Zhao, J. Feng, Q. Huo, N. Melosh, G.H. Fredrickson, B.F. Chmelka, G.D. Stucky, Science 279 (1998) 548.
[58] Y. Han, N. Li, L. Zhao, D. Li, X. Xu, S. Wu, Y. Di, C. Li, Y. Zou, Y. Yu, F.S. Xiao, Journal of Physical Chemistry B 107 (2003) 7551–7556.
[59] F. Zhang, Y. Yan, H. Yang, Y. Meng, Y. Meng, C. Yu, B. Tu, D. Zhao, Journal of Physical Chemistry B 109 (2005) 8723–8732.
[60] M. Kruk, L. Cao, Langmuir 23 (2007) 7247–7254.
[61] P.E. Boahene, K.K. Soni, A.K. Dalai, J. Adjaye, Applied Catalysis A: General 402 (2011) 31–40.
[62] A. Galarneau, B. Lefevre, H. Cambon, B. Coasne, S. Valange, Z. Gabelica, J.P. Bellatd, F. Di Renzoa, Studies in Surface Science and Catalysis 174 (2008) 957–960.
[63] N. Calin, A. Galarneau, T. Cacciaguerra, R. Denoyel, F. Fajula, Comptes Rendus Chimie 13 (2010) 199–206.
[64] F. Kleitz, F. Berube, C.M. Yang, M. Thommes, Studies in Surface Science and Catalysis 170 (2007) 1843–1849.
[65] J. Barrault, J.M. Tatibouet, N. Papayannakos, Comptes Rendus de l'Academie des Sciences – Series IIC: Chemistry 3 (2000) 777–783.
[66] C.E. Webster, R.S. Drago, Michael C. Zerner, Journal of the American Chemical Society 120 (1998) 5509–5516.
[67] P. Massa, F. Ivorra, P. Haure, R. Fenoglio, Journal of Hazardous Materials 190 (2011) 1068–1073.
[68] A. Quintanilla, S. Garcia-Rodriguez, C.M. Dominguez, S. Blasco, J.A. Casas, J.J. Rodriguez, Applied Catalysis B: Environmental 111–112 (2012) 81–89.
[69] A. Quintanilla, J.A. Casas, J.J. Rodriguez, Applied Catalysis B: Environmental 93 (2010) 339–345.
[70] H.T. Gomes, S.M. Miranda, M.J. Sampaio, J.L. Figueiredo, A.M.T. Silva, J.L. Faria, Applied Catalysis B: Environmental 106 (2011) 390–397.
[71] L. Hu, X. Yang, S. Dang, Applied Catalysis B: Environmental 102 (2011) 19–26.